Supplementary Information

Stimuli-responsive lipid-based magnetic nanovectors increase apoptosis in glioblastoma cells through synergic intracellular hyperthermia and chemotherapy

Christos Tapeinos [a,†,], Attilio Marino [a,†,*], Matteo Battaglini [a,b], Simone Migliorin [c], Rosaria Brescia [d], Alice Scarpellini [d], César De Julián Fernández [e], Mirko Prato [f], Filippo Drago [g], Gianni Ciofani [a,c,*]*

[a] Smart Bio-Interfaces, Istituto Italiano di Tecnologia, Pontedera (Pisa), 56025 Italy

[b] The Biorobotics Institute, Scuola Superiore Sant'Anna, Pontedera (Pisa), 56025 Italy

[c] Department of Mechanical and Aerospace Engineering, Politecnico di Torino, Torino, 10129 Italy

[d] Electron Microscopy Facility, Istituto Italiano di Tecnologia, Genova, 16163 Italy

[e] Istituto dei Materiali per l'Elettronica e il Magnetismo, Consiglio Nazionale delle Ricerche - CNR, Parma, 43124 Italy.

[f] Materials Characterization Facility, Istituto Italiano di Tecnologia,Genova, 16163 Italy

[g] Nanochemistry Department, Istituto Italiano di Tecnologia, Genova, 16163 Italy

Transmission electron microscopy (TEM)

The morphological characterization of the lipid-based magnetic nanovectors (LMNVs) was performed using a JEM-1011 TEM (W filament), operated at 100 kV. Each sample was sonicated for a few minutes to avoid the presence of aggregates. 5 µl of the solution were dropped onto an ultrathin carbon-coated Cu grid. The samples were stained with 1% uranyl acetate for 30 s before analysis. The images presented in Figure S1 depict LMNVs stained with uranyl acetate at two different magnifications. In both images the spherical morphology of the nanovectors is evident, as well as the encapsulated superparamagnetic iron oxide nanoparticles (SPIONs; dark electron-dense spots).

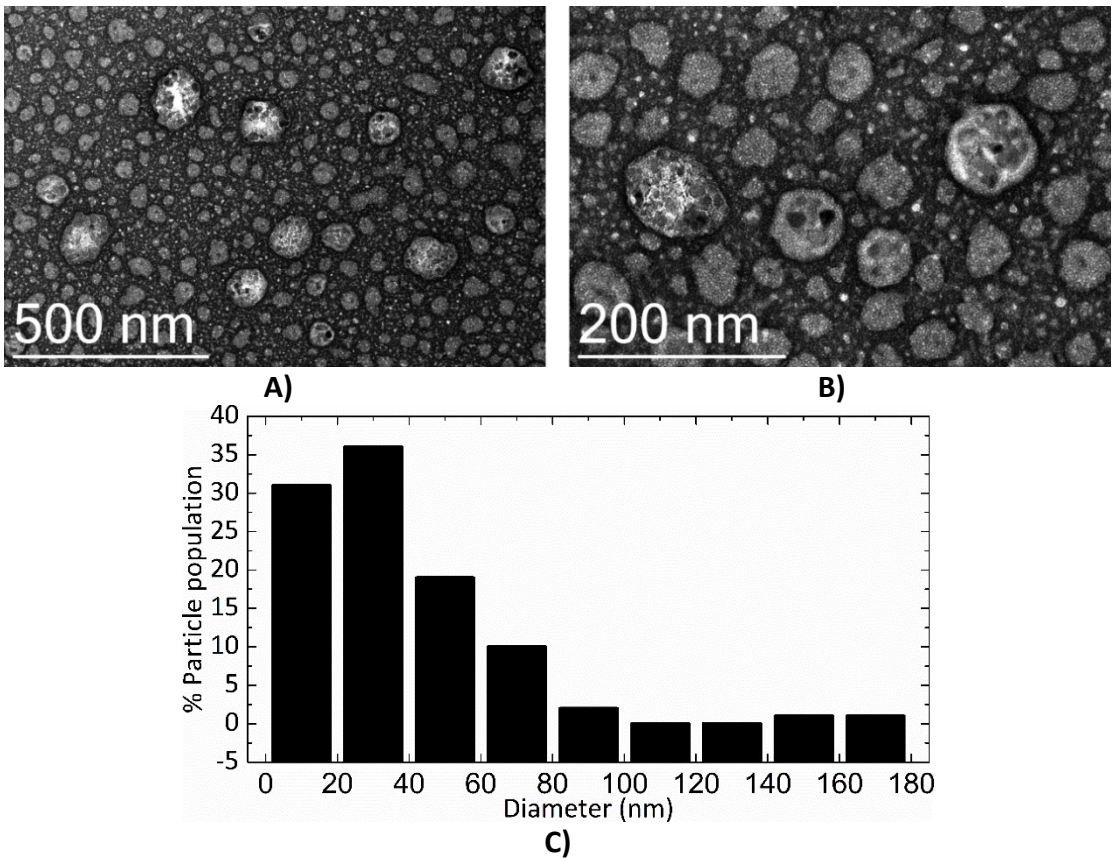

Figure S1. A) and B) bright field (BF) TEM images of LMNVs at two different magnifications, where the distribution and the morphology of the nanovectors can be seen. The dark spots (higher electron density) inside the lipid matrix (grey color) depict SPION aggregates; C) size distribution of the nanovectors after analysis with ImageJ, where it can be seen that the majority of the particles present a diameter size less than 80 nm.

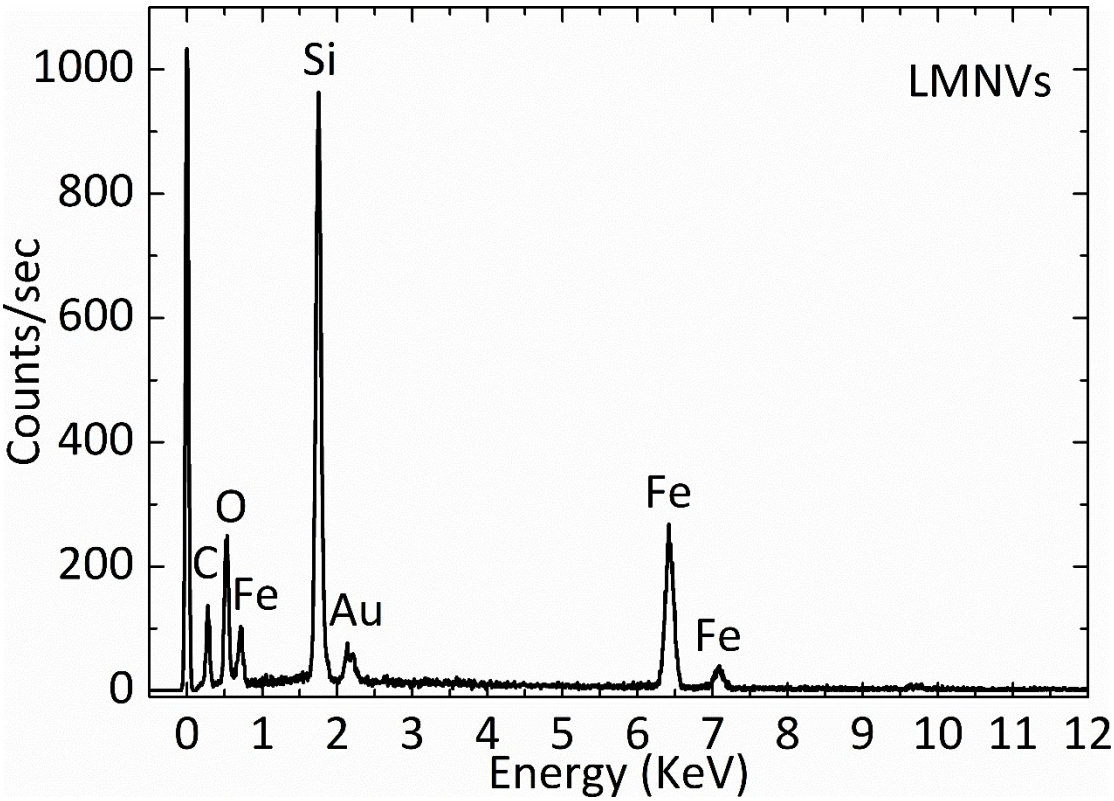

Figure S2. Electron dispersive X-ray analysis spectrum of the LMNVs, where the basic elements of each of their components (lipid matrix and Fe_3O_4 nanoparticles) are presented. The corresponding percentages of each element by weight are C: 24.60 %, O: 35.13 %, Fe: 40.14 %. Si and Au peaks were excluded from the calculation of the percentages.

LMNV stability studies and protein corona formation

The stability of the nanoparticles in various media (H_2O, Dulbecco's modified Eagle media -DMEM-, and DMEM + 10% fetal bovine serum -FBS-), and at various time points (1, 6, and 24 h) was assessed using dynamic light scattering. The used concentration of the LMNVs was 100 μg/ml.

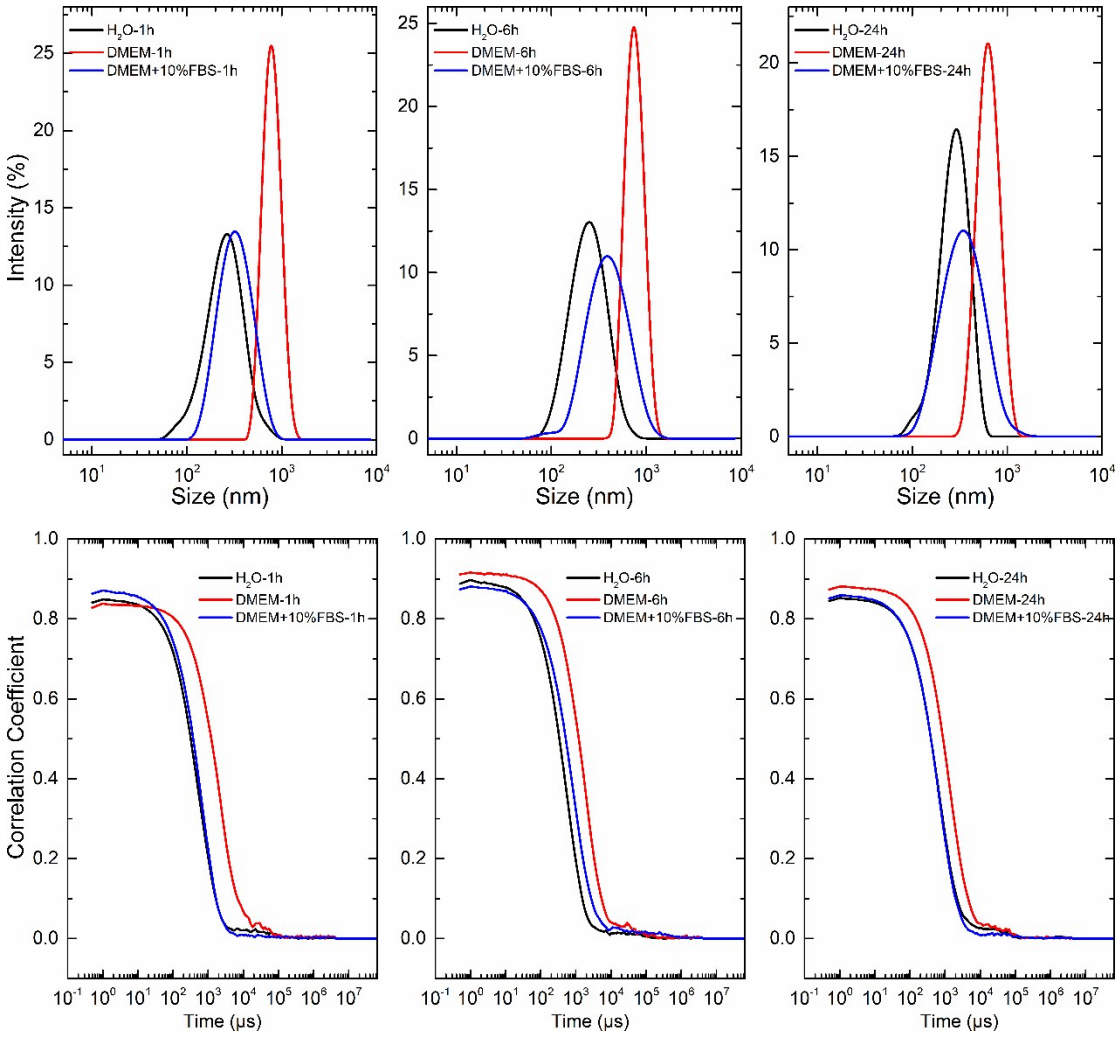

Figure S3. Stability studies (intensity *vs.* size on the top and correlograms at the bottom) of the LMNVs in different dispersants (H_2O, DMEM and DMEM+10%FBS) and at different time points (1, 6 and 24 h). On top: DLS graphs presenting the size distribution of the particles in various solvents. The black and the blue curves correspond to the size distribution of the LMNVs in water and in DMEM+10% FBS, respectively, and it is evident that in water and in DMEM+10% FBS the size is stable. The shifted red curve on the right represents the LMNVs in DMEM, demonstrating a higher size that can be attributed to aggregation. At the bottom: The correlograms at 4, 6, and 24 h show increased stability and relatively small size when the LMNVs are in water or in DMEM+10% FBS (low decay times and well-fitted sigmoidal curves), while they present a larger size (red curve shifted to higher decay times) and increased sedimentation at 4 h (increased spikes when decay time is more than 10^4 μs) when dispersed in DMEM.

Nanoparticle tracking analysis

Using nanoparticle tracking analysis (NTA) we were able to quantify the concentration of the particles as well as to study their behavior in various solvents under flow. NTA can be considered more accurate compared to dynamic light scattering, due to the fact that records the movement of each individual particle and is able to provide a more accurate size distribution (after applying the Stoke-Einstein equation) in relation to the number of particles, and not the intensity of the particles as DLS does. Although for all the measurements 100 μg/ml of LMNVs were used, it can be observed that the number of particles *per* milliliter is not the same for the different used dispersants, and this can be probably attributed to inaccuracies during the serial dilutions that were performed. Nevertheless, the number of particles is high enough in order to provide accurate and reproducible results. The NTA graphs and their corresponding results that are provided in Table S1 are in close agreement with the DLS results, although significant changes are observed concerning the mean diameter. It has to be noted that, although NTA can be used as a complementary technique for the characterization of the size distribution, of the polydispersity, and of the relative stability of the nanoparticles, it should not be confused with the results provided by the DLS, because as we said above, DLS uses the particle intensity to calculate the mean size, while NTA uses particle number.

According to the results provided in Table S1, LMNVs present an average hydrodynamic diameter of approximately 270 nm in water, 118 nm in DMEM, and 104 nm in DMEM+10%FBS. Although the LMNVs in water should present lower hydrodynamic diameters, closer to those ones that DLS gives (ca. 100 nm), they do not. This is probably attributed to some aggregates that were formed before the insertion of the sample in the NT analyzer, allowing the observation of a second population which shifts the hydrodynamic diameter towards higher values. Herein, it has to be noted that an average size of 100 nm from DLS does not exclude the presence of a population with a larger diameter, that cannot be seen in the Gaussian distribution of the intensity *vs.* size (H_2O/24h, Figure S3, top graph), due to the limitations of the DLS. However, the elevated baseline in the correlogram in Figure S3 (H_2O/24h, bottom graph) suggests that a population with larger diameter, probably due to a small aggregation of the sample, is present. This aggregation can explain the higher mean diameter of the LMNVs in water that is given from the NTA (266.6 ± 9.8 nm). When changing dispersant, a peak at 350 nm (DMEM, Figure S4), similar to that one in H_2O can be also observed, but in this case the mean diameter (118.6 ± 7.0 nm) is not affected as much as in the case of water (266.6 ± 9.8 nm), and this is attributed to the fact that there is a higher concentration of particles with a size of approximately 100 nm that makes the larger population less significant. This larger population of approximately 350 nm is not so evident in the case of DMEM+10%FBS, and this can be probably attributed to the protein corona formation that increases the stability of the LMNVs by reducing their aggregation, probably due to steric hindrances. In conclusion, it is safe to say that the majority of the LMNVs presents increased size stability under flow when a biologically relevant medium (DMEM+10%FBS) is used, suggesting a prolonged circulation time in media with high ionic strength like body fluids.

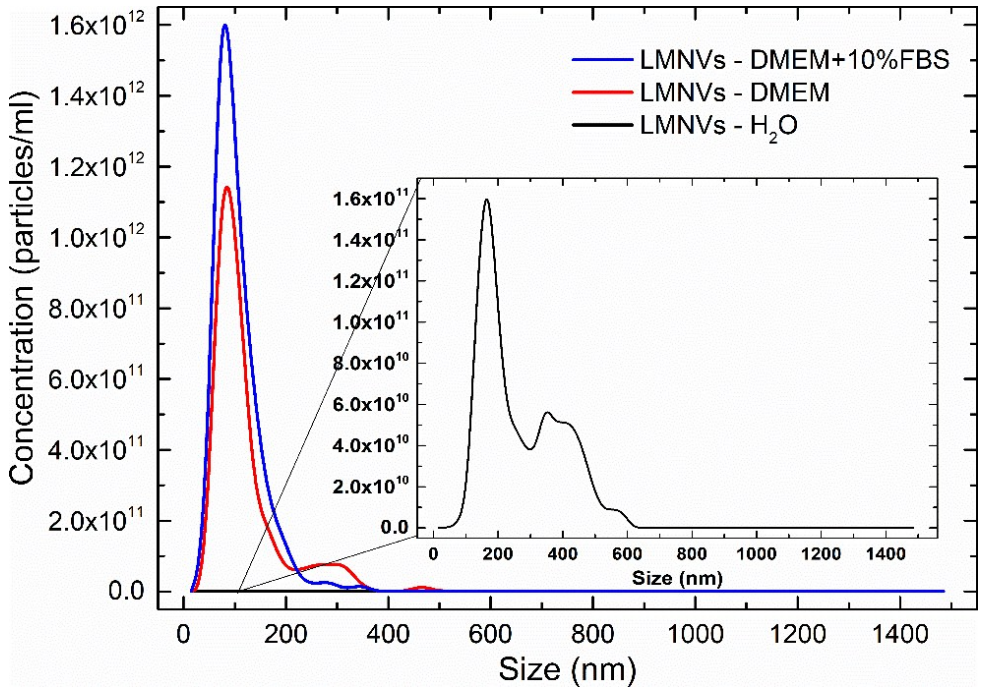

Figure S4. Nanoparticle tracking analysis graphs presenting the behavior of the LMNVs in different dispersants (H_2O, DMEM and DMEM+10%FBS) after 24 h under flow. The peak at approximately 100 nm, for DMEM and DMEM+10% FBS, and at approximately 200 nm for LMNVs in water, shows the average hydrodynamic diameter of the particles after 24 h. In plain DMEM and in water a second peak at 350 nm and at 400 nm, respectively, represents populations with a larger size, while in DMEM+10%FBS this population is not significantly high, demonstrating the increased stability of the nanoparticles probably due to the protein corona formation.

Table S1. Information resulting from the nanoparticle tracking analysis of the LMNVs in different dispersants after 24 h.

	LMNVs in H_2O	**LMNVs in DMEM**	**LMNVs in DMEM+10%FBS**
Mean	266.6 ± 9.8 nm	118.6 ± 7.0 nm	104.3 ± 2.2 nm
Mode	171.7 ± 5.9 nm	83.7 ± 0.9 nm	80.3 ± 0.9 nm
SD	119.8 ± 7.1 nm	64.6 ± 9.8 nm	42.9 ± 1.4 nm
***D10**	139.9 ± 5.4 nm	66.7 ± 0.4 nm	64.7 ± 0.9 nm
***D50**	229.2 ± 10.3 nm	97.5 ± 2.9 nm	91.0 ± 1.6 nm
***D90**	445.0 ± 17.3 nm	215.4 ± 33 nm	159.8 ± 7.7 nm

**The D10, D50 and D90 values (D-values) represent diameters at which, correspondingly, 10%, 50% and 90% of a sample mass is comprised of smaller particles.*

Magnetic hyperthermia during release studies

The magnetic hyperthermia during the release studies was also recorded. The results that are depicted in Figure S5 present the response of the particles subjected to alternating magnetic field (AMF) at each time point (4, 24, 72, and 168 h) and for various conditions, including the treatment at different pH (4.5 and 7.4), the treatment with or without hydrogen peroxide (H_2O_2), as well as a combination of them.

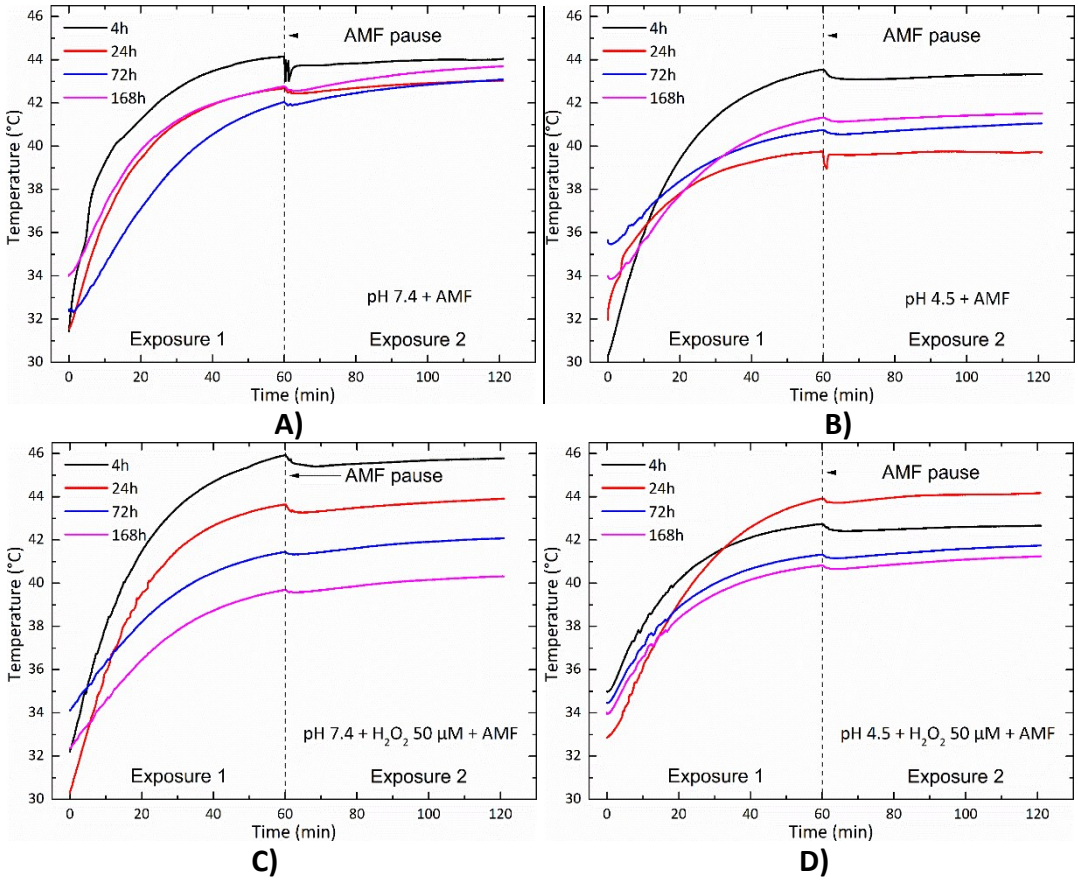

Figure S5. Temperature profiles during the release studies of temozolomide under various treatments (different pH, increased H_2O_2 concentration that simulates the overexpressed ROS in glioblastoma, and under treatment with an alternating magnetic field with the subsequent increase in temperature) and at different time points. A) pH 7.4 + AMF, B) pH 4.5 + AMF, C) pH 7.4 + H_2O_2 + AMF, D) pH 4.5 + H_2O_2 + AMF. The samples were exposed to a magnetic field of 20 mT at a frequency of 752 KHz for 2 h, with a 1 min pause after the first hour. The concentration of the samples was 2.4 mg/ml. The differences in the temperature profiles can be attributed to the precipitation of the particles during the time and/or to a small deformation of the particles because of the applied treatments.

Evaluation of the specific absorption rate (SAR) and of the intrinsic loss power (ILP)

In order to evaluate the thermal response of the LMNVs under the influence of an external magnetic field, SAR and ILP were calculated after exposure of the LMNVs to three different field intensities and at two different frequencies. In order to accurately evaluate the SAR and ILP values, the experimental conditions were different than those ones that were used for the loading and release studies. The SAR and ILP studies were performed in a smaller volume (100 µl of final volume inside a typical NMR tube) instead of the 1 ml final volume inside a Nalgene tube that was instead used for the release studies. Since the magnetic field inside a coil is not homogeneous and exponentially decays when diverging from the center, and since we cannot focus the magnetic field into a specific volume, we used the NMR tubes and 100 µl of volume, aiming at exploiting the maximum possible field intensity that is not affected by the distance from the center of the coil, as well as to have reproducible conditions. In addition, all the calculations were made for an increment of temperature of 6°C, that corresponded to the difference from 37°C (body temperature) to 43°C (mild hyperthermia). The results are given in Table S2.

Table S2. Specific absorption rate and intrinsic loss power of LMNVs under treatment at various field frequencies and intensities

Sample	Field (mT)	Field (kA/m)	Frequency (KHz)	dT (° C)	dt (sec)	dT/dt	Mass of pure Fe from ICP (mg/L)	Specific Absorption Rate (W/g)	Intrinsic Loss Power (nHm^2/Kg)
Fe_3O_4 - 3 nm	15	12.0	750	0.44	20	0.022	0.16	583	5.40
Fe_3O_4 - 3 nm	17	13.6	750	0.45	20	0.022	0.16	583	4.21
Fe_3O_4 - 3 nm	20	16.0	750	0.47	20	0.023	0.16	611	3.18
Fe_3O_4 - 3 nm	15	12.0	525	0.35	20	0.018	0.16	462	4.28
Fe_3O_4 - 3 nm	17	13.6	525	0.37	20	0.019	0.16	483	3.48
Fe_3O_4 - 3 nm	20	16.0	525	0.52	20	0.026	0.16	678	3.53
LMNVs	15	12.0	750	0.70	20	0.035	0.16	911	8.43
LMNVs	17	13.6	750	0.67	20	0.034	0.16	880	6.34
LMNVs	20	16.0	750	0.98	20	0.080	0.16	1282	6.68
LMNVs	15	12.0	525	0.62	20	0.031	0.16	811	7.51
LMNVs	17	13.6	525	0.54	20	0.027	0.16	706	5.09
LMNVs	20	16.0	525	1.03	20	0.052	0.16	1345	7.00
*LMNVs	20	16.0	750	0.55	20	0.028	0.15	755	3.93
*LMNVs	20	16.0	525	0.41	20	0.021	0.15	571	2.98

** All the measurements in Table S2 were performed in NMR tubes with an internal diameter of 4.14 mm and a final volume of 100 µl, except the last two measurements that were performed during the release studies in a Nalgene tube with an internal of diameter 10 mm and a final volume of 1 ml. SAR and ILP values were calculated using the mass of pure Fe as it was calculated by ICP.*

Evaluation of LMNV cell up-take by flow cytometry

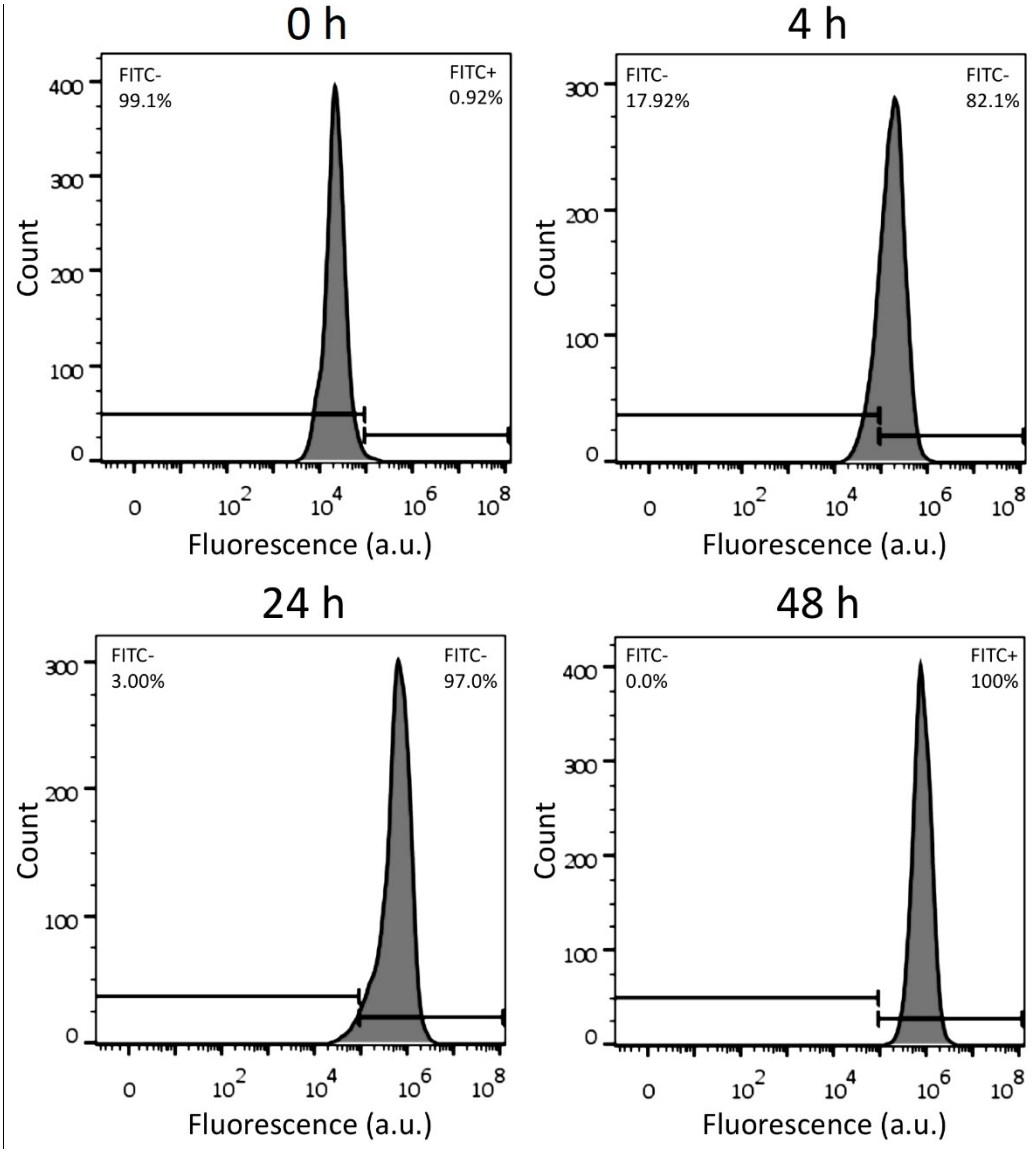

Figure S6. Flow cytometry graphs presenting the progressive internalization of DiO-stained LMNVs in U-87 MG cells (λex = 488 nm; 485 nm < λem < 565 nm). At 0 h the fluoresence intensity is less than 104 a.u., while after 4, 24 and 48 h of incubation the fluorescence intenisy of the treated U-87 MG cell population is gradually shifted to higher fluorescent values, suggesting a higher amount of internalized DiO-stained LMNVs.

Metabolic activity assay

The WST-1 assay was used to assess the metabolic activity of the cells treated with plain nanovectors (LMNVs), with nanovectors loaded with temozolomide (TMZ-LMNVs) as well as with free temozolomide (TMZ) (Figure S7A). In addition, WST-1 was also used to assess the metabolic activity of the LMNVs (400 µg/ml) without and with (+AMF) exposure to an alternating magnetic field (Figure S7B). The results are presented below in Figure S7A and S7B, respectively.

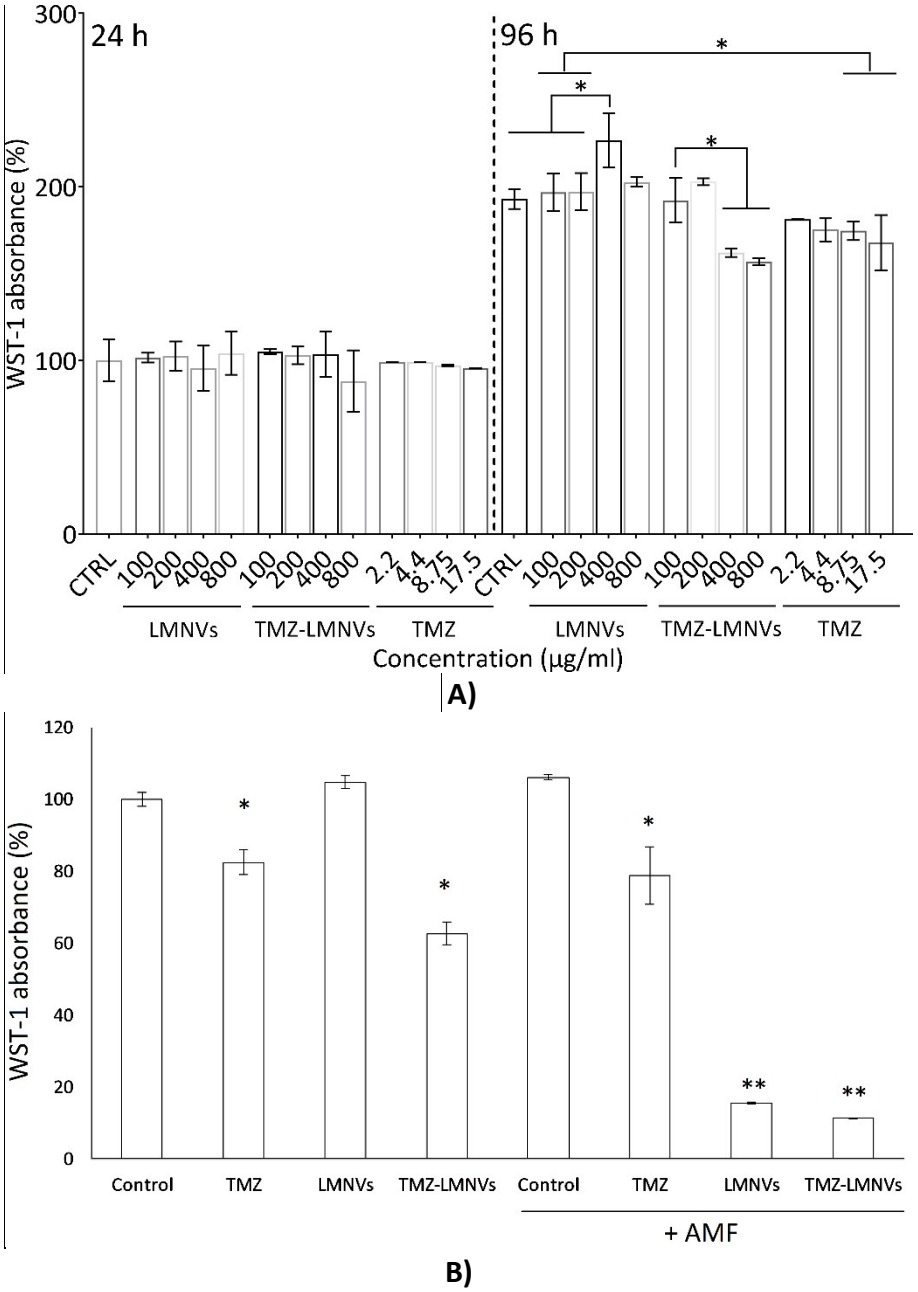

Figure S7. A) Analysis of cancer cell metabolism after treatment with plain LMNVs, free TMZ, and TMZ-LMNVs, at various concentrations (100 - 800 µg/ml of nanovectors and 2.2 - 17.5 µg/ml of free TMZ) and at two time points (24 and 96 h); B) metabolic activity of cells following treatment with plain LMNVs, free TMZ (8.75 µg/ml) and TMZ-LMNVs (400 µg/ml), with and without exposure to AMF (20 mT, 750 KHz) after 96 h. Absorbance levels are normalized for the non-incubated non-stimulated control cultures. * $p < 0.05$, ** $p < 0.005$.

Assessment of apoptosis by flow cytometry

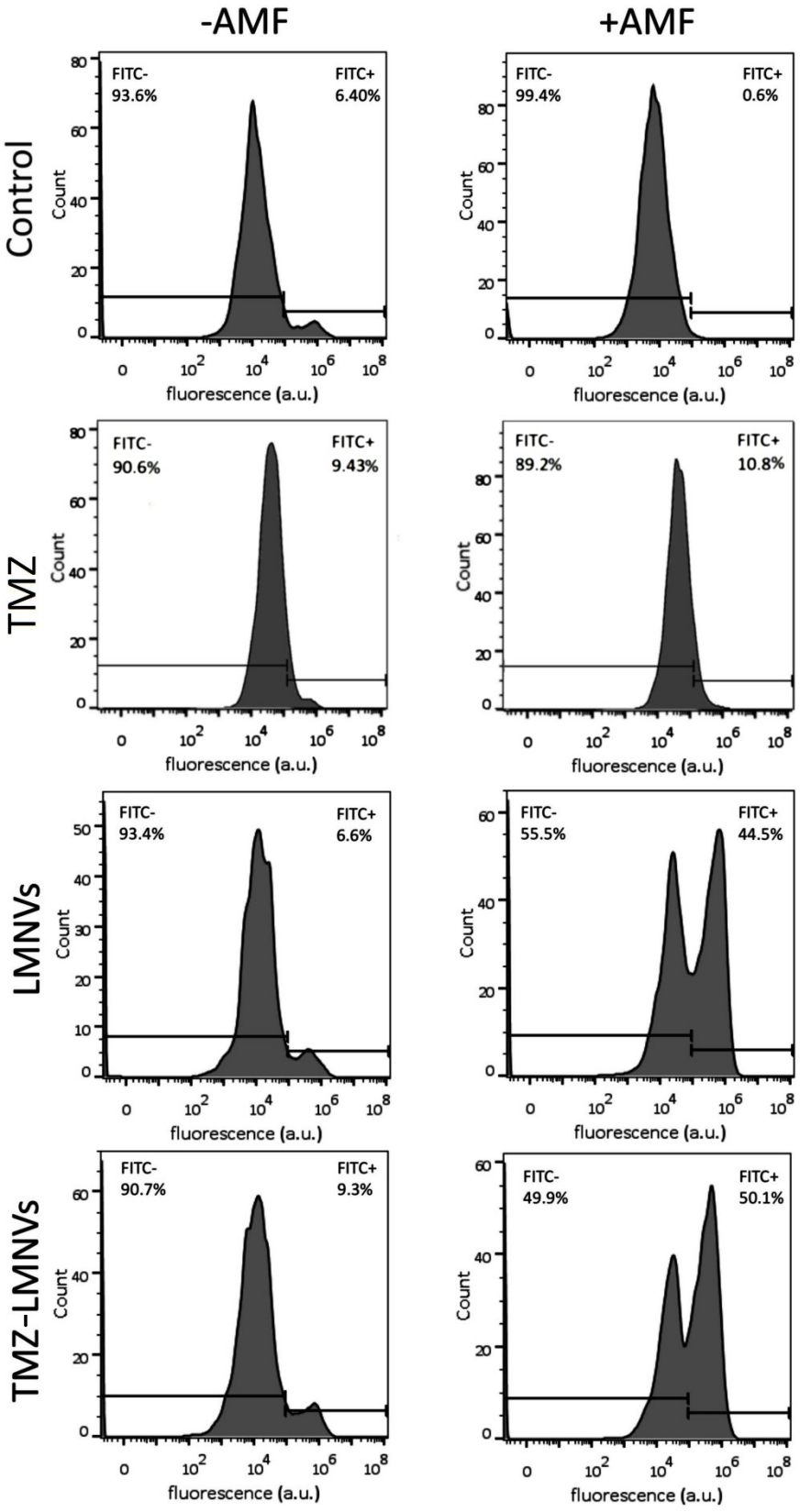

Figure S8. Graphs reporting the fluorescence emission of annexin V-FITC stained cells in the different experimental groups. Data of fluorescence emission in LMNVs+AMF and in TMZ-LMNVs+AMF are characterized by a bimodal distribution highlighting two populations of cells, negative and positive for annexin V-FITC, which respectively indicate viable and apoptotic cells.

Spectral imaging of DiD-stained LMNVs

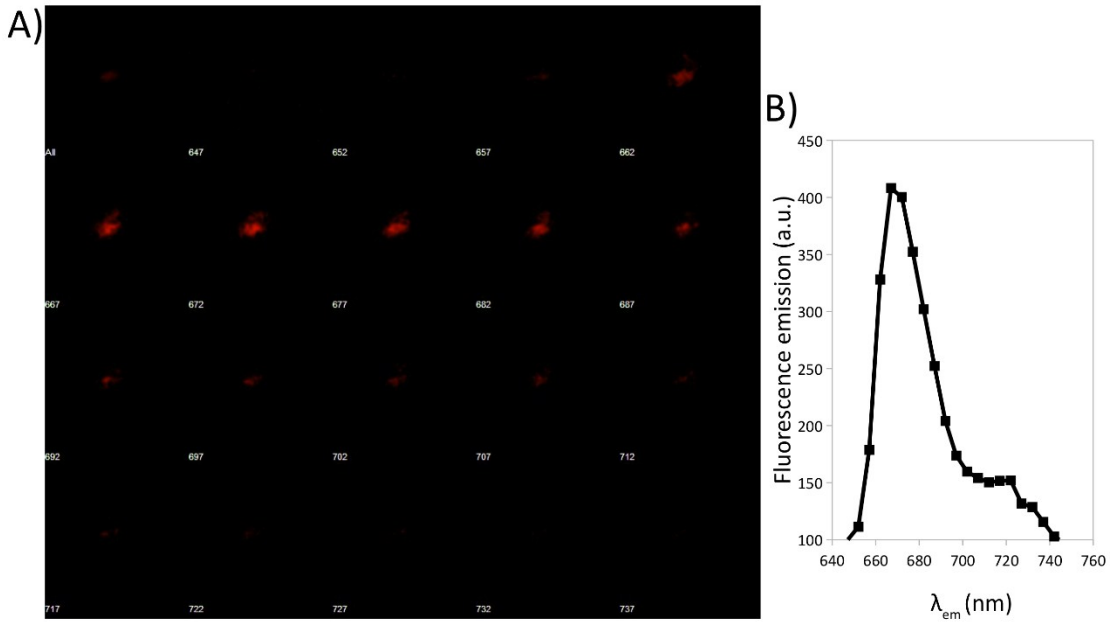

Figure S9. A) CLSM imaging of a single DiD-stained LMNV at different emission wavelengths; B) emission spectrum of a single DiD-stained LMNV.